Proceedings of GT2006
ASME Turbo Expo 2006: Power for Land, Sea and Air
May 8-11, 2006, Barcelona, Spain

GT2006-90045

SHORT LENGTH-SCALE ROTATING STALL INCEPTION IN A TRANSONIC AXIAL COMPRESSOR – CRITERIA AND MECHANISMS

Chunill HAH[1], Jörg BERGNER[2] and Heinz-Peter SCHIFFER[2]

[1]NASA Glenn Research Center,
MS 5-11, Cleveland, Ohio 44135
[2]Technische Universität Darmstadt
D-64287 Darmstadt, Germany

ABSTRACT

The current paper reports on investigations aimed at advancing the understanding of the flow mechanism that leads to the onset of short-length scale rotating stall in a transonic axial compressor. Experimental data show large oscillation of the tip clearance vortex as the rotor operates near the stall condition. Inception of spike-type rotating stall is also measured in the current transonic compressor with high response pressure transducers. Computational studies of a single passage and the full annulus were carried out to identify flow mechanisms behind the spike-type stall inception in the current transonic compressor rotor. Steady and unsteady single passage flow simulations were performed, first to get insight into the interaction between the tip clearance vortex and the passage shock. The conventional Reynolds-averaged Navier-Stokes method with a standard turbulence closure scheme does not accurately reproduce tip clearance vortex oscillation and the measured unsteady pressure field. Consequently, a Large Eddy Simulation (LES) was carried out to capture more relevant physics in the computational simulation of the rotating stall inception. The unsteady random behavior of the tip clearance vortex and it's interaction with the passage shock seem to be critical ingredients in the development of spike-type rotating stall in a transonic compressor. The Large Eddy Simulation was further extended to the full annulus to identify flow mechanisms behind the measured spike-type rotating stall inception. The current study shows that the spike-type rotating stall develops after the passage shock is fully detached from the blade passages. Interaction between the tip clearance vortex and the passage shock creates a low momentum area near the pressure side of the blade. As the mass flow rate decreases, this low momentum area moves further upstream and reversed tip clearance flow is initiated at the trailing edge plane. Eventually, the low momentum area near the pressure side reaches the leading edge and forward spillage of the tip clearance flow occurs. The flows in the affected blade passage or passages then stall. As the stalled blade passages are formed behind the passage shock, the stalled area rotates counter to the blade rotation just like the classical Emmon's type rotating stall. Both the measurements and the computations show that the rotating stall cell covers one to two blade passage lengths and rotates at roughly 50% of the rotor speed

INTRODUCTION

The current design trend in high-speed axial flow compressors is to increase aerodynamic loading on each blade row. With increased aerodynamic blade loading, it is critical to maintain a suitable operating range. Many research programs aimed at understanding and controlling stall inception in compression systems have been reported. It is well known that there are two distinctive routes to rotating stall in a compressor. The long-scale or modal inception has been extensively studied and is believed to be well understood (for example, Moore and Greitzer [1986], and Camp and Day [1998]). On the other hand, short-length scale or spike type inception is not fully understood, especially in high-speed compressors. While modal inception can be successfully described without considering details of the flow inside the blade passages, spike inception analysis requires understanding of detailed flow structures inside the blade passages because the spike disturbance is comparable in scale to the mean velocity through the compressor. Recently, many studies have been reported on the role of flow structure in spike type rotating stall inception in low-speed compressors (Outa et al. [1994], He and Ismael [1997], Hoing et al. [1998], Saxer-Felici et al. [1998], Hah et al. [1999], Gong et al. [1999], and Vo et al. [2005]). Vo et al. [2005] investigated criteria for spike-

initiated rotating stall inception in a subsonic compressor. Their comprehensive and thorough study indicates that leading edge tip clearance flow spillage and net upstream mass flow at the trailing edge of the blade tip are two criteria for rotating stall inception.

The overall process of rotating stall inception is not as well understood in high-speed compressors as it is in low speed compressors. It is generally known that rotating stall precedes complete disruption of engine operation in the surge cycles. Few experimental or analytical studies have been reported on rotating stall inception in a high-speed compressor (for example, He and Ismail [1997], Hah and Rabe [2001]). He and Ismail [1997] numerically simulated stall inception in an isolated blade row of NASA's Rotor 67 using a partial annulus domain of ten blade passages and periodicity conditions to approximate the full annulus. Their study indicates that an isolated blade row with supersonic inflow tends to stall in a one-dimensional "surge-like" pattern without first experiencing rotating stall. One possible explanation of this behavior is that supersonic inlet flow might allow information to propagate only in one circumferential direction upstream of the blade row. Hah and Rabe [2001] performed an unsteady Reynolds-averaged Navier-Stokes analysis over the full annulus of an isolated transonic compressor rotor. The numerically produced rotating signal in terms of axial velocity was very similar to the measured rotating stall signals from high-response pressure transducers mounted upstream of the rotor. The numerical analysis revealed that the axial positions of shocks detached from the rotor blades vary from blade to blade, and that this non-uniform shock front produces the rotating stall signal.

The main objective of the current study is to computationally reproduce measured rotating stall inception in a transonic compressor. The numerical results are examined in detail to understand the relevant flow mechanisms.

TEST ROTOR AND TEST FACILITY

The compressor stage under investigation in this study is the front stage of a high-pressure compressor in a commercial turbofan. A series of transonic compressor rotors have been designed and tested at the Department of Gas Turbine, Flight and Space Propulsion at the Technical University of Darmstadt, Germany. The design parameters of the tested rotor are given in Table 1. Figure 1 shows a front view of the rotor with the full-annulus grid. Further details of the test facility and applied measurement techniques are given by Bergner et al. [2005]. Measured pressure rise characteristics of the rotor at the design rotor speed are shown in Fig. 2 along with computed pressure characteristics to be discussed in later sections of this paper. All the numerical simulations were performed for the isolated rotor configuration. The current compressor stage has a relatively large space between the rotor and the stator and any upstream influence of the stator was not included in the numerical simulation.

Steady and unsteady single-passage Reynolds averaged Navier-Stokes computations were performed and the calculated pressure rise characteristics in the stable and stalled operations are also shown in Fig. 2. Additionally a single passage Large Eddy Simulations were performed in the stable operating range and the results are also given in Fig. 2. To understand stall inception, the Large Eddy Simulation was also performed over the full annulus in stall. An instantaneous solution during stall with the full annulus LES is also shown in Fig. 2.

NUMERICAL PROCEDURE

Steady and unsteady Reynolds-averaged Navier-Stokes (RANS) methods and a Large Eddy Simulation (LES) method were applied in the present study. The steady and unsteady three-dimensional RANS procedures were applied to obtain steady and unsteady flow fields at various operating conditions. The unsteady RANS solutions were obtained to study oscillation of the tip clearance vortex and its interaction with the passage shock at various operating conditions and also to obtain instantaneous flow structures during stall inception. A modified two-equation turbulence model was used for turbulence closure in the RANS methods. The LES procedure was applied primarily to explore additional unsteady flow features that are relevant to rotating stall inception but cannot be calculated accurately with RANS procedures. With spatially filtered Navier-Stokes equations, the subgrid-scale stress tensor term must be modeled properly for the closure of the governing equations. A Smagorinsky-type eddy-viscosity model was used for the subgrid stress tensor, and the standard dynamic model by Germano et al. [1991] was applied.

In the current study, the governing equations are solved with a pressure-based implicit method using a fully conservative control volume approach. A third-order accurate interpolation scheme is used for the discretization of convection terms and central differencing is used for the diffusion terms. The method is of second-order accuracy with smoothly varying grids. For the time-dependent terms, an implicit second-order scheme is used and a number of sub-iterations are performed at each time step. Details of the RANS method and applications to transonic flows are given by Hah and Wennerstrom [1991].

The computational grid for a single blade passage consists of 198 nodes in the blade-to-blade direction, 77 nodes in the spanwise direction, and 200 nodes in the streamwise direction. The inflow boundary was located 6 average blade heights upstream of the rotor leading edge and the outflow boundary was located one blade height from the trailing edge. The rotor tip clearance geometry is accurately represented by 28 nodes in the blade-to-blade direction, 16 nodes in the spanwise direction, and 140 nodes in the streamwise direction. For the full-annulus LES simulation, only 100 nodes are used in the blade-to-blade direction to reduce the turn around time. The I-grid topology is used to reduce grid skewness and a single-block grid is used. All the computations were performed with NASA's Columbia super

computer system, which allows parallel computation with up to 512 computers.

Standard boundary conditions for an isolated rotor were applied at the boundaries of the computational domain. Circumferentially averaged static pressure at the casing was specified to control the mass flow rate. The current investigation focuses on the initial stall inception process. Therefore, the exit flow condition was not varied dynamically. Non-reflecting boundary conditions were applied at the inlet and the exit boundaries.

FLOW STRUCTURES FROM SINGLE-PASSAGE ANALYSIS

Changes in flow structure during the transition from stable operation to stall were first studied with a conventional RANS method on a single blade passage. Although the single-passage analysis cannot simulate rotating stall, similar changes in flow structure can occur in a single blade passage during actual rotating stall inception. The calculations were performed by incrementally increasing reference backpressure and enforcing circumferential periodicity conditions. Calculated pressure rise characteristics are shown in Fig. 2. The operating point marked as “in stall” in Fig. 2 represents an instantaneous flow solution, not a steady converged solution, since a steady converged solution cannot be obtained in stall.

Figure 3 shows a comparison of measured and calculated endwall static pressure distributions at the design and near-stall conditions. The numerical solution in Fig. 3 referred to as “near stall” corresponds to the maximum possible backpressure that permits a steady solution. The overall measured flow structures at different operating conditions are well reproduced by the computations.

To examine changes in flow structure during stall with a single passage simulation, an instantaneous flow field was calculated after stall and compared with the near stall solution. Figure 4 shows Mach number contours, velocity vectors, and particle traces at these two operating conditions. Before stall, the shock is still attached at the leading edge of the blade and no forward spillage of tip clearance flow is observed near the leading edge. In stall, however, the passage shock is completely detached and velocity vectors near the leading edge show forward spillage of tip clearance flow just below the tip section. Also, the particle traces show reversed tip clearance flow at the trailing edge plane. As shown in Fig. 4, the two criteria for spike-type rotating stall inception proposed by Vo et al. [2005] apply to the current transonic compressor rotor. The main mechanisms behind these stall criteria are the formation and forward movement of low momentum fluid near the pressure side.

As the compressor operation moves toward the stall condition, the flow field becomes highly unsteady due to oscillations of passage shock and the tip leakage vortex and interactions between them. Figure 5 compares relative RMS values of endwall static pressure. The relative RMS values are RMS values divided by local average pressure. The results in Fig. 5 indicate that the unsteadiness in the flow field near stall is mainly caused by oscillation of the tip leakage vortex and its interaction with the passage shock. Both the measurement and the calculation show that the unsteadiness due to pure shock oscillation is much smaller than that due to the tip vortex oscillation. Although the relative RMS distribution from the RANS simulation shows a similar qualitative trend, the unsteadiness due to vortex oscillation is under predicted.

Figure 6 compares instantaneous endwall static pressure distributions from the measurement and the RANS calculation. The measured instantaneous pressure shows much greater variation in both the shape and magnitude of the tip leakage core vortex compared to the RANS simulation.

It is generally believed that the tip leakage vortex and its interaction with the passage shock are major ingredients in spike-type rotating stall inception. Therefore, a more realistic representation of the tip leakage vortex and its random interaction with the passage shock is highly desirable for the computational study of rotating stall inception in a transonic compressor. A LES simulation was performed in this study for a single passage in order to compare with the RANS simulation. Figure 7 shows relative RMS values of endwall static pressure from the LES simulation. Fig. 8 shows instantaneous static pressure distributions from the LES simulation. The pressure oscillation from the single passage analysis shown in Fig. 8 is rather random at this operating condition and any distinct frequency could not be clearly identified. Compared to the RANS results, LES seems to reproduce the flow physics more realistically. The current study focuses on unsteady motion of the tip leakage vortex and its random interaction with the passage shock, which occurs away from the blade surface. With the currently applied computational grid, the turbulent flow structure inside the blade boundary layer might not be fully resolved. However, the vortex behavior away from the solid blade and endwall is modeled more realistically with LES.

The instantaneous LES solutions were averaged over 500 time steps and the averaged flow solutions are shown in Fig. 9. The time-averaged near stall solution seems to show more flow features and agrees better with the measured flow field. Particle traces from the time-averaged solution are shown in Fig. 10. Results in Figures 9 and 10 show formation of the tip clearance core vortex, induced vortex, and low momentum area near the pressure side of the blade. As previous studies have indicated (for example, Hoffmann and Ballmann [2003], Hah et al. [2004]), the tip clearance core vortex moves radially inward at about 20% chord from the leading edge. Flows originating from the blade tip section between 20% and 60% chord cross over the core vortex and form the induced vortex very close to the casing. The induced vortex was also previously observed by Van Zante et al. [2000]. The low momentum area (flow blockage) forms just behind the induced vortex. The particle traces at in-stall operation in Fig. 4c show that the induced vortex reaches the leading edge of the adjacent blade, and then forward spillage of the tip clearance flow occurs. Detailed examination of the instantaneous solutions indicate

that when the back pressure is raised beyond the stable steady solution limit for the current rotor, reversed tip clearance flow at the trailing edge plane occurs just before the tip clearance flow spillage at the leading edge.

FULL ANNULUS ANALYSIS / SPIKE-TYPE ROTATING STALL INCEPTION

Unsteady flow analyses over the full annulus were performed to understand how spike-type rotating stall inception occurs in a transonic compressor rotor. In a real compressor rotor, rotating stall initiates in a particular blade passage or passages. Some unpublished experimental data indicate that the circumferential location of rotating stall inception is not directly related to minor variations in blade geometry. Also, spike type rotating stall inception was observed experimentally in an isolated transonic rotor configuration with identical blade geometry and with a uniform inflow condition. To achieve a realistic numerical simulation of rotating stall inception, the numerical procedure with any closure modeling should allow variation of instantaneous flow field among blade passages even with identical blade geometries and a uniform inflow condition. It is believed that vortex shedding, passage shock oscillation, and tip clearance vortex oscillation occur randomly and that the phase and magnitude of these oscillations varies among blade passages even with uniform inflow conditions.

Therefore, the inception of spike-type rotating stall can be realistically calculated if the random oscillation of the tip clearance vortex and the passage shock, and the associated vortex shedding, are accurately represented in the numerical procedure. Because LES realistically calculates the random oscillation of the tip clearance vortex and its interaction with the passage shock, the currently applied LES method was applied to the analysis of rotating stall inception.

Figure 11 shows measured histories of casing static pressure at 100% axial chord upstream of the leading edge. The measurement indicates that rotating stall develops over 1 to 2 rotor revolutions and that the rotating stall cell rotates at about half of the rotor speed.

Figure 12 shows measured casing pressure distributions during the development of rotating stall. The measured endwall pressure distribution is the pressure field recorded as the rotor blades pass under the assembly of high-response pressure transducers. Although the time-lapsed plots of wall pressure do not give instantaneous structures of the flow field, many important features of the unsteady flow field can be observed. The rotating stall cell is observed over two rotor revolutions in the time-lapsed plots of the casing pressure distribution. Also, the measured stall cell appears about twice as large in the circumferential direction than it actually is because the rotating stall cell moves at half of the rotor speed.

Calculated instantaneous Mach number and static pressure contours just below the blade tip section at the beginning of stall inception are shown in Fig. 13, which also correspond to the operating point of -4 in Fig. 11. The sonic line in Fig.13 shows that the passage shock is fully detached from the leading edge over the full annulus. As the stall cell forms behind the sonic plane, the stalled area can move in the circumferential direction just like in classical subsonic rotating stall. In Fig. 14, instantaneous velocity vectors around stalled blade passages and around healthy passages are shown. In the stalled blade passage, tip clearance flow is reversed at the trailing edge plane and forward spillage of the tip clearance flow is observed at the leading edge. Outside the rotating stall cell, none of these two phenomena are present. Further examination of the instantaneous flow fields leading to stall inception reveals the sequence of rotating stall inception. First, the passage shock is fully detached. Second, the tip clearance vortex trajectory in the stalled passage moves sufficiently forward to the leading edge. During this time, tip clearance flow at the trailing edge plane reverses its direction and impinges on the pressure side of the adjacent blade. Finally, forward spillage of the tip clearance flow occurs near leading edge of the blade. The current numerical simulation shows that random movement of the tip clearance vortex and its interaction with the passage shock is the main mechanism of spike-type rotating stall inception in the current transonic compressor rotor. Instantaneous tip clearance core vortex structures just before stall inception from the full-annulus simulation are shown in Fig. 15. The instantaneous tip clearance core vortex structure varies from passage to passage, which leads to spike type stall inception on a particular blade passage or passages.

Calculated static pressure and velocity vectors just below the tip section are shown in Fig. 16 after the rotating stall cell is fully established, which correspond to the operating point of 0 in Fig. 11. The calculated rotating stall cell covers roughly two blade passages in the circumferential direction, in agreement with the measurements, and about 10 to 20% span. In Fig. 17, instantaneous Mach number contours at the 50% axial chord cross plane are shown. The results in Fig. 17 show that the stall cell rotates opposite to the direction of blade rotation and it extends up to 20% blade height from the casing. Further examination of the movement of the rotating stall cell shows that its rotational speed is about 50% of the rotor speed.

CONCLUDING REMARKS

The occurrence of short length scale rotating stall inception in a transonic compressor rotor was studied with steady and unsteady flow simulations. The following observations were made from the current study.

The flow field becomes unsteady as the rotor operates near stall. The unsteadiness is due to oscillation of tip clearance vortices and their interactions with the passage shocks. Both the measurements and calculations show that the unsteadiness due to tip clearance vortex oscillation is much larger than that due to pure shock oscillation. Therefore, the interaction between the tip clearance vortex and the passage shock is an inherently unsteady phenomenon in a transonic compressor.

The spike-type rotating stall develops after the passage shock is fully detached from the blade leading edge over the full annulus.

The mechanism of spike-type rotating stall cell inception in the current transonic rotor can be described as follows: First, The passage shock is fully detached. Second, the tip clearance vortex trajectory moves toward the leading edge in a particular passage during its random oscillation and reversed tip clearance flow develops at the trailing edge plane. Finally, forward spillage of tip clearance flow develops at the leading edge as the induced vortex reaches the leading edge along with low momentum fluid near the pressure side.

Both the measurements and the numerical simulations show that the circumferential size of the rotating stall cell is about two blade passages and that the cell rotates at about 50% of the rotor speed.

ACKNOWLEDGMENTS

The authors would like to acknowledge the contribution of J. Loellbach of ICOMP during the current investigation.

REFERENCES

Bergner, J., Hennecke, D. K., and Hah, C., 2005, "Tip-Clearance Variations of an Axial High-Speed Single-Stage Transonic Compressor," ISABE Paper ISABE-2005-1096.

Camp, T. R. and Day, I. J., 1998, "A Study of Spike and Modal Stall Phenomena in a Low-Speed Axial Compressor," ASME Journal of Turbomachinery, Vol. 120, pp.393-401.

Germano, M., Piomelli, U., Moin, P., and Cabot, W. H., 1991, "A Dynamic Subgrid-Scale Eddy-Viscosity Model," Journal of Fluid Mechanics, Vol. A3, pp.170-176.

Gong, Y., Tan, C. S., Gordon, K A., and Greitzer, E. M., 1999, "A Computational Model for Short Wavelength Stall Inception and Development in Multi-Stage Compressors," ASME Journal of Turbomachinery, Vol. 121, pp.726-734.

Hah, C. and Rabe, D. C., 2001, "Role of Tip Clearance Flows on Flow Instability in Axial Flow Compressors," ISABE Paper 2001-1223.

Hah, C., Rabe, D. C., and Wadia, A. R., 2004, "Role of Tip-Leakage Vortices and Passage Shock in Stall Inception in a Swept Transonic Compressor Rotor," ASME Paper GT2004-53867.

Hah, C. and Wennerstrom, A. J., 1991, "Three-Dimensional Flow Fields Inside a Transonic Compressor with Swept Blades," ASME Journal of Turbomachinery, Vol. 113, No. 1, pp. 241-251.

He, L. and Ismael, J. O., 1997, "Computations of Blade Row Stall Inception in Transonic Flows," ISABE Proceedings, pp.697-707.

Hoying, D. A., Tan, C. S., Vo, H. D., and Greitzer, E. M., 1998, "Role of Blade Passage Flow Structures in Axial Compressor Rotating Stall Inception," ASME Paper 98-GT-588.

Hoffmann W. H. and Ballmann, J., 2003, "Some Aspects of Tip Vortex Behavior in a Transonic Turbocompressor," ISABE Paper 2003-1223.

Moore, F. K. and Greitzer, E. M., 1986a, "A Theory of Post-Stall Transients in Axial Compression Systems: Part 1 - Development Equations," ASME Journal of Engineering for Gas Turbines and Power, Vol. 108, pp. 68-76.

Moore, F. K. and Greitzer, E. M., 1986b, "A Theory of Post-Stall Transients in Axial Compression Systems: Part 2 - Application," ASME Journal of Engineering for Gas Turbines and Power, Vol. 108, pp. 231-239.

Outa, E., Kato, D., and Chiba, K., 1994, "A N-S Simulation of Stall Cell Behavior in a 2-D Compressor Rotor-Stator System at Various Loads," ASME Paper 94-GT-257.

Saxer-Felici, H. M., Saxer, A. P., Inderbitzin, A., and Gyarmathy, G., 1998, "Prediction and Measurement of Rotating Stall Cells in an Axial Compressor," ASME Paper 98-GT-67.

Van Zante, D. E., Strazisar, A. J., Wood, J. R., Hathaway, M. D., Okiishi, T. H., 2000, "Recommendations for Achieving Accurate Numerical Simulation of the Tip Clearance Flows in Transonic Compressor Rotors," ASME Journal of Turbomachinery, Vol. 122, pp. 733-742.

Vo, H. D., Tan, C. S., and Greitzer, E. M., 2005, "Criteria for Spike Initiated Rotating Stall," ASME Paper GT2005-68374.

Pressure ratio	1.5
Corrected mass flow rate	16.0 kg/s
Corrected tip speed	398 m/s
Inlet relative Mach number at tip	1.35
Inlet relative Mach number at hub	0.70
Shaft speed	20,000 rpm
Tip diameter	0.38 m
Rotor mean aspect ratio	0.94
Rotor solidity (hub/mid/tip)	1.9/1.5/1.2

Table 1: Rotor design parameters.

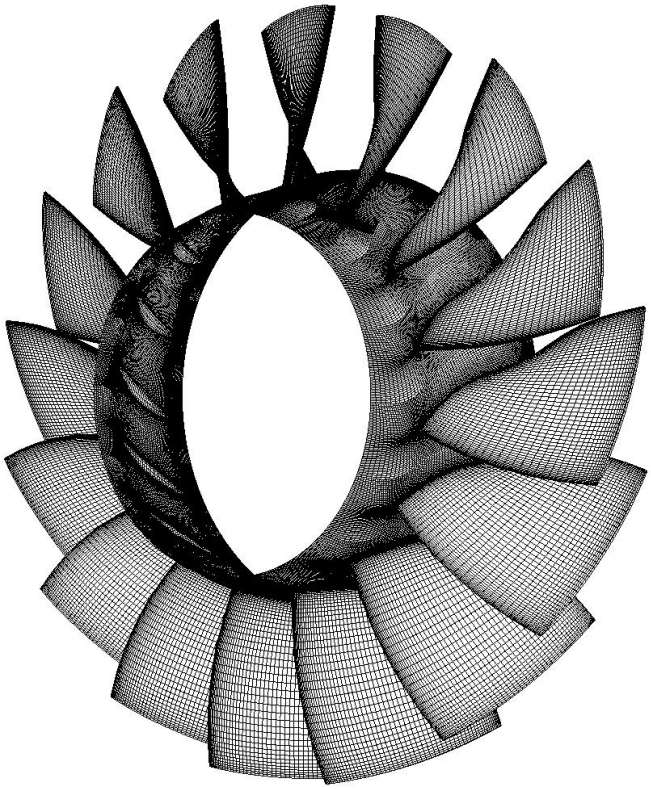

Figure 1: Front view of rotor.

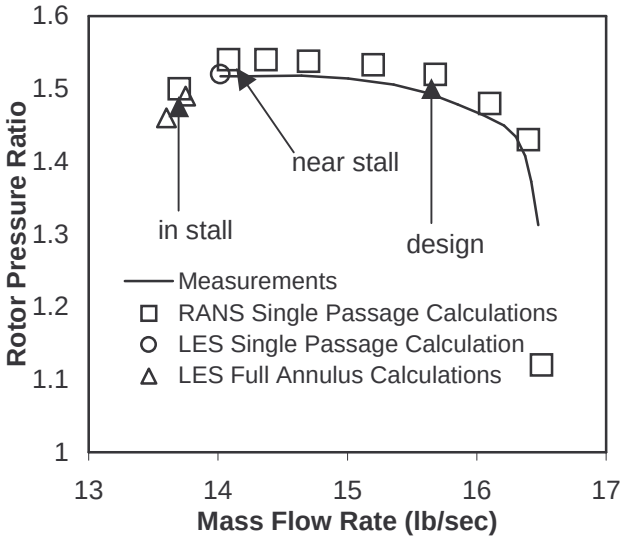

Figure 2: Pressure rise characteristics of the rotor.

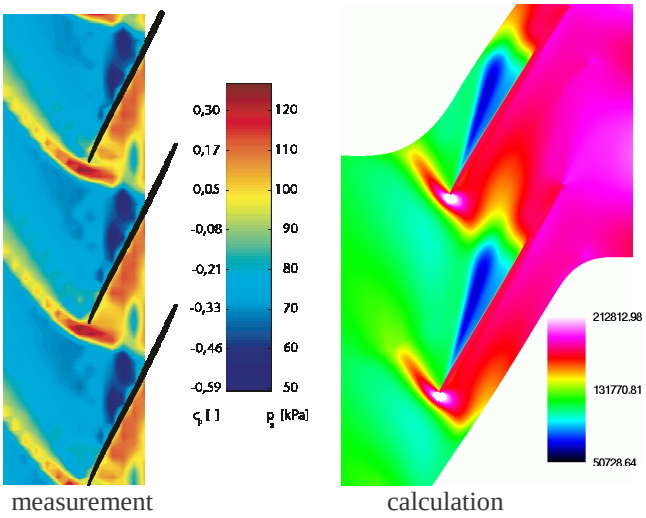

Figure 3a: Comparison of casing static pressure distribution at design condition.

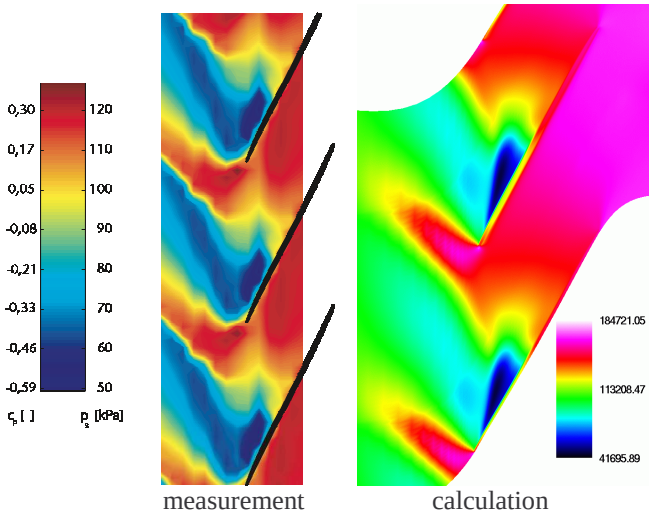

Figure 3b: Comparison of casing static pressure distribution near stall.

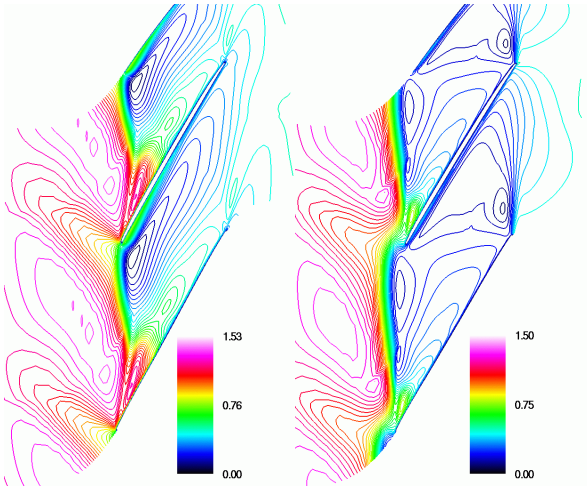

near stall in stall

Figure 4a: Comparison of Mach number distribution at rotor tip.

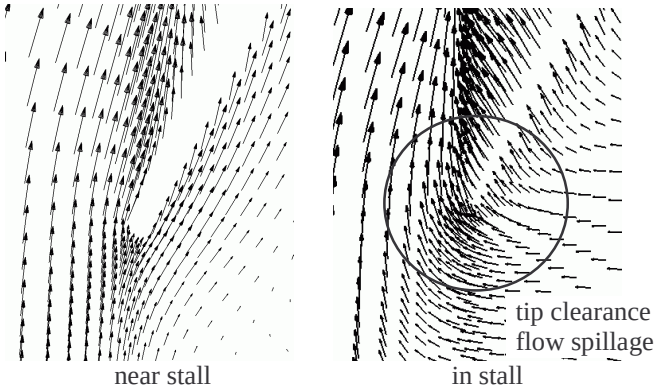

near stall in stall

Figure 4b: Comparison of velocity vectors at rotor tip.

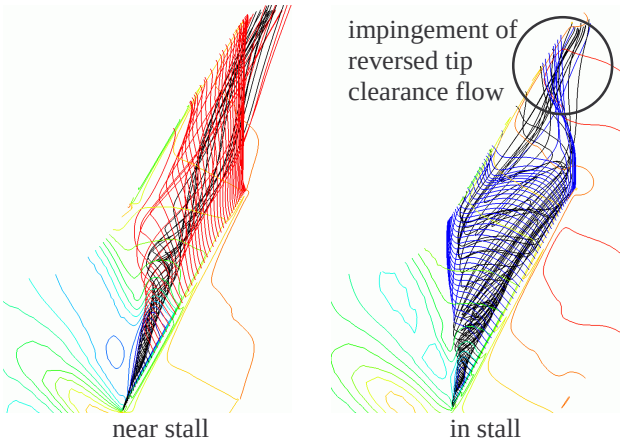

near stall in stall

Figure 4c: Comparison of particle traces at rotor tip.

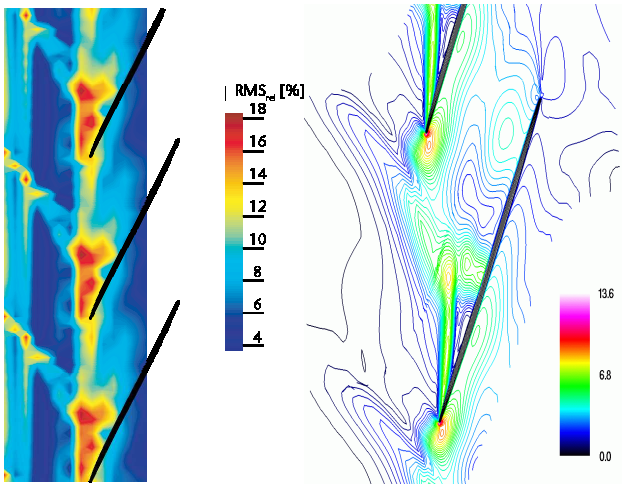

measurement RANS calculation

Figure 5: Comparison of measured and RANS relative RMS casing static pressure distributions near stall.

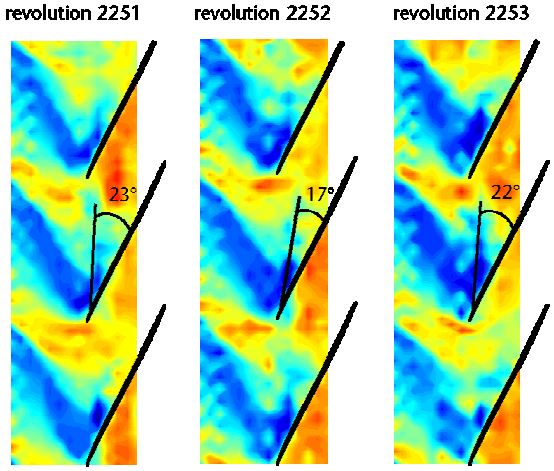

Figure 6a: Measured instantaneous endwall static pressure distributions near stall.

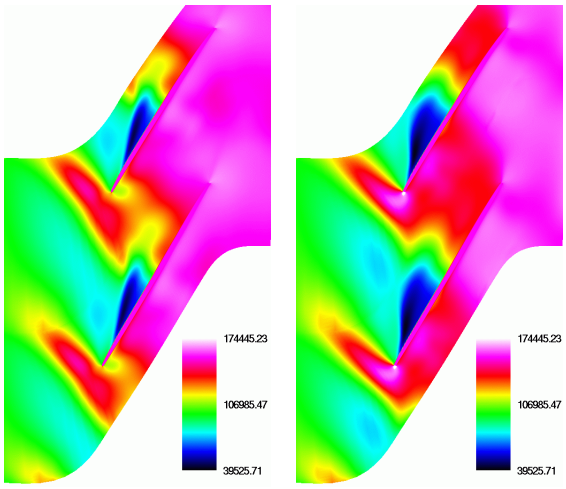

time step 1 time step 2

Figure 6b: Calculated instantaneous casing static pressure distributions from RANS near stall.

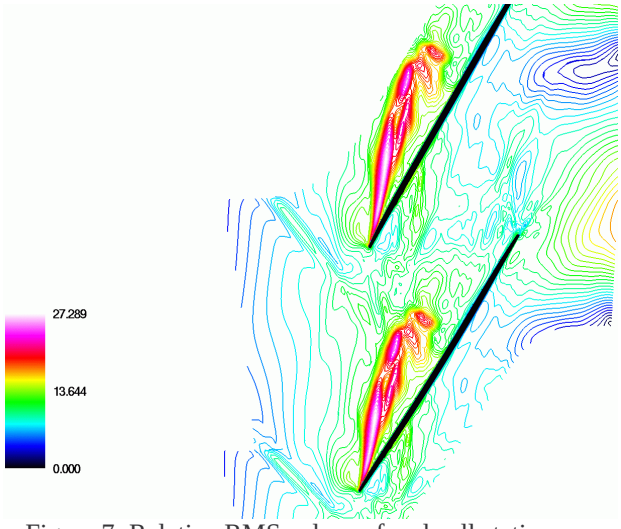

Figure 7: Relative RMS values of endwall static pressure from LES near stall from single-passage calculation.

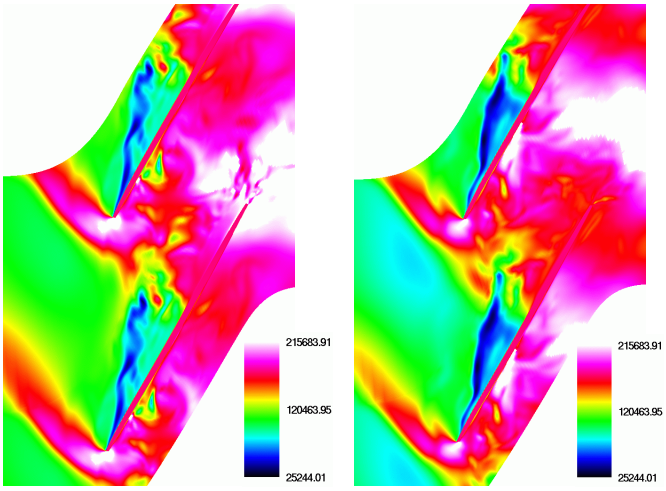

time step 1 time step 2

Figure 8: Calculated instantaneous casing static pressure from LES near stall.

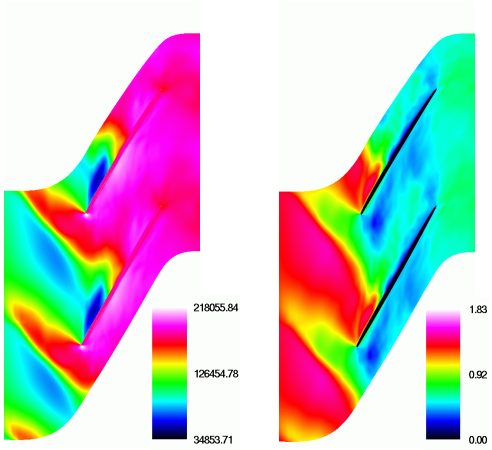

static pressure Mach number

Figure 9: Casing static pressure and Mach number distribution at 98% span from time-averaged LES solution near stall.

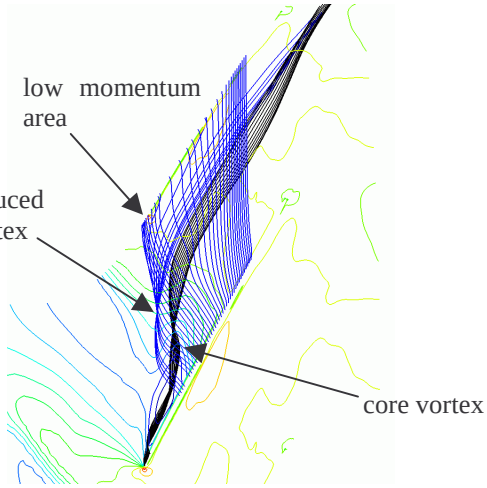

Figure10: Particle traces from time-averaged LES solution near stall.

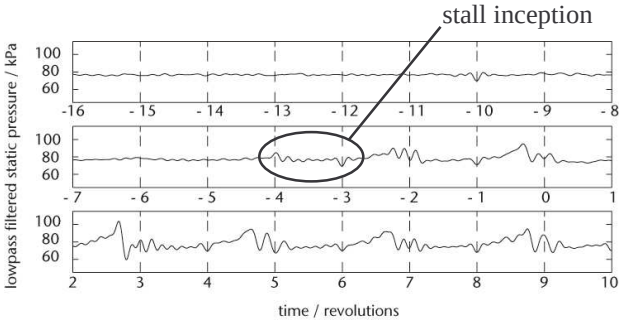

Figure 11: History of casing static pressure at 100% axial chord upstream of the leading edge.

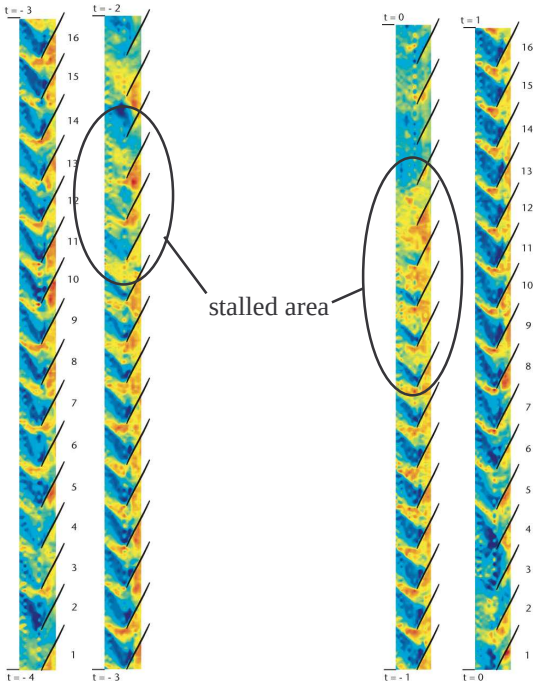

from rotation –4 to –2 from rotation –1 to 1

Figure 12: Time-lapsed distribution of measured casing static pressure during rotating stall inception.

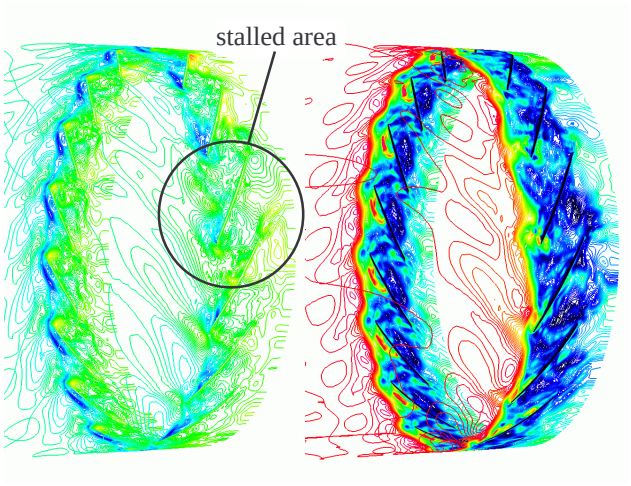

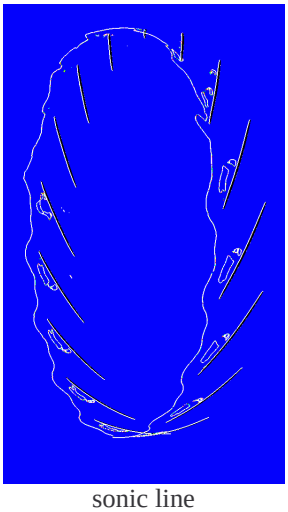

Figure 13: Instantaneous distribution of static pressure, Mach number, and sonic line at 98% span at the beginning of rotating stall inception.

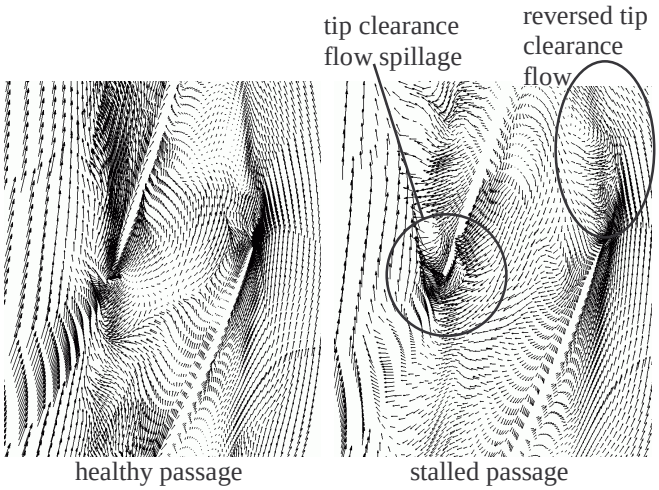

Figure 14: Velocity vectors, 98% span at the beginning of rotating stall inception.

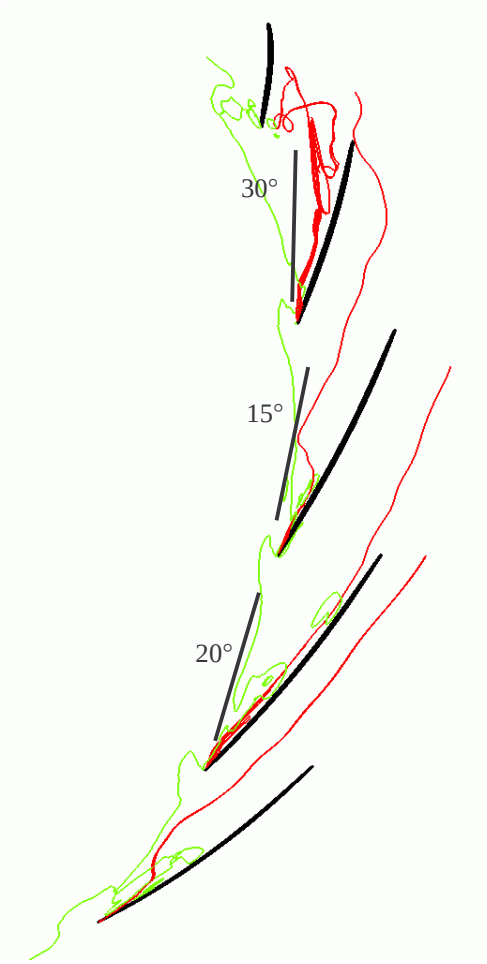

Figure 15: Instantaneous tip clearance vortex traces just before stall inception.

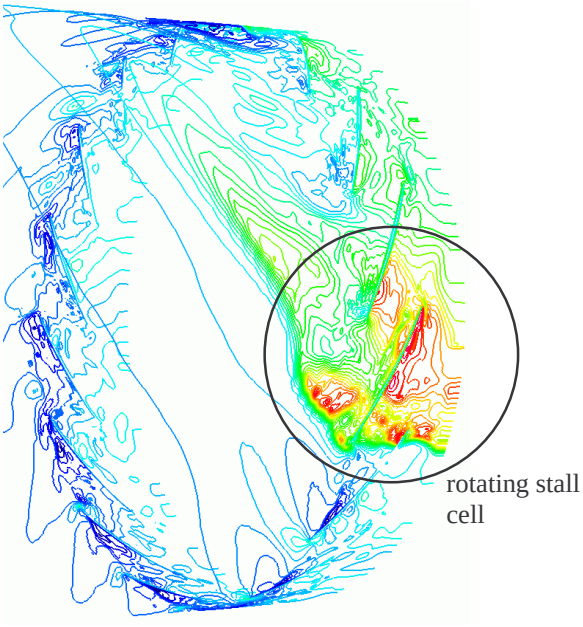

pressure

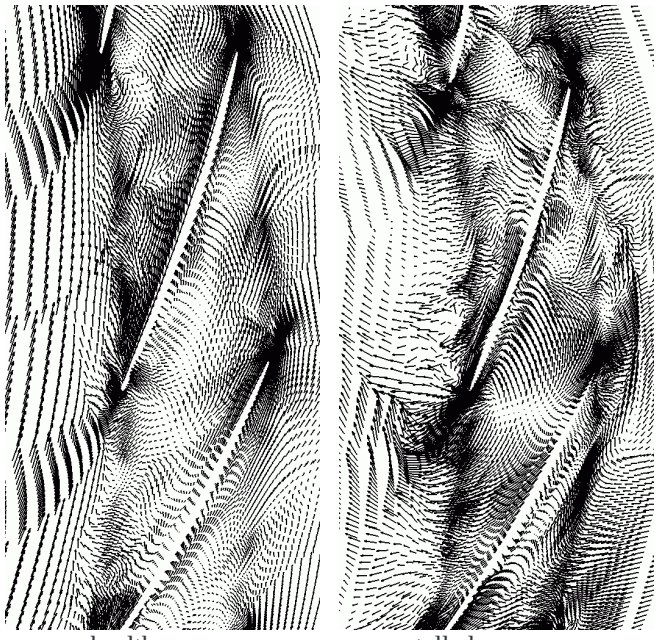

healthy passage stalled passage

Figure 16: Instantaneous distribution of static pressure and velocity vectors at 98% span as rotating stall develops.

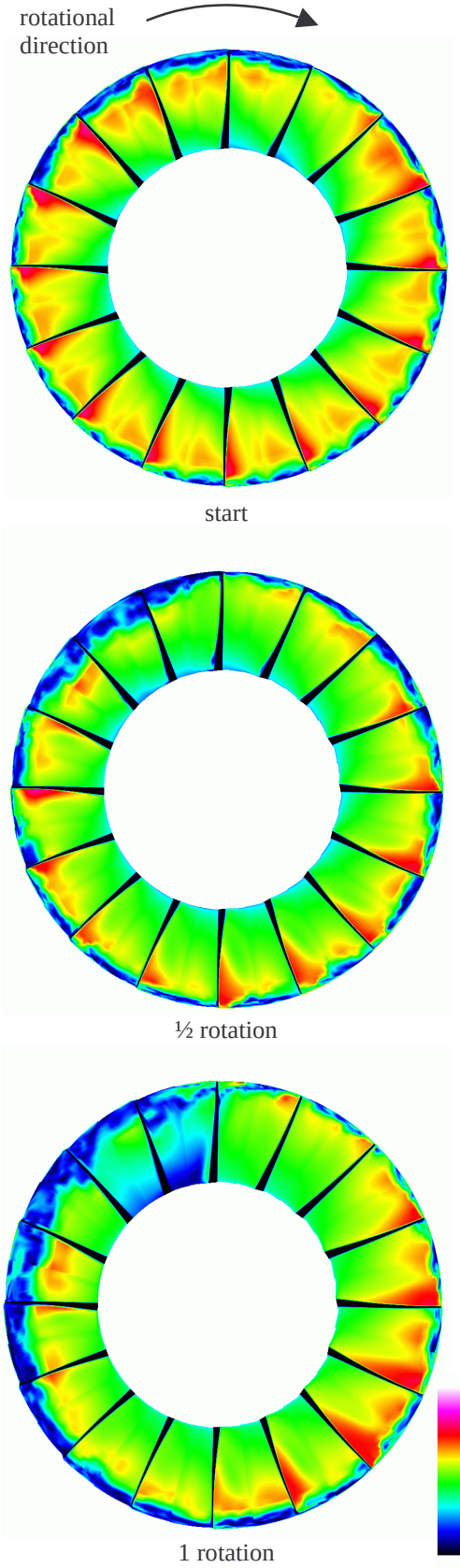

start

½ rotation

1 rotation

Figure 17: Changes in instantaneous Mach number contours at 50% axial chord.